

Library Copy
a. A31L3 R04

SECURITY INFORMATION

C.2
Copy 44
RM SL52C12

NACA

RESEARCH MEMORANDUM

for the

Bureau of Aeronautics, Department of the Navy

TOTAL-PRESSURE-RECOVERY CHARACTERISTICS OF A MODEL

OF THE MCDONNELL XF3H-1 INLETS AND FOREBODY

IN A FREE JET AT A MACH NUMBER OF 1.55

By Charles F. Merlet and Howard S. Carter

Langley Aeronautical Laboratory
Langley Field, Va.

CLASSIFICATION CHANGED

To UNCLASSIFIED

By authority of NASA memo Date Feb 18, 1963

s/Boyd E. Myers II

This material contains information affecting the National Defense of the United States within the meaning of the espionage laws, Title 18, U.S.C., Secs. 793 and 794, the transmission or revelation of which in any manner to unauthorized person is prohibited by law.

**NATIONAL ADVISORY COMMITTEE
FOR AERONAUTICS**

ARR - 5-1-63

WASHINGTON
MAR 12 1952

~~CONFIDENTIAL~~

CLASSIFICATION CHANGED
UNCLASSIFIED
Authority of 18 USC 793, 794
Approved by William Date 2/18/63



NATIONAL ADVISORY COMMITTEE FOR AERONAUTICS

RESEARCH MEMORANDUM

for the

Bureau of Aeronautics, Department of the Navy

TOTAL-PRESSURE-RECOVERY CHARACTERISTICS OF A MODEL

OF THE MCDONNELL XF3H-1 INLETS AND FOREBODY

IN A FREE JET AT A MACH NUMBER OF 1.55

By Charles F. Merlet and Howard S. Carter

SUMMARY

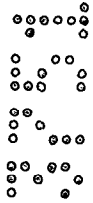
Free jet tests, at a Mach number of 1.55 and at 0° angle of attack and yaw, were made of a model of the inlets and forebody of the McDonnell XF3H-1 airplane with the original and two alternate nose shapes. The pressure measurements made at the inlet and after diffusion showed high-frequency oscillations throughout the mass-flow range tested. The average total-pressure recovery after diffusion ranged from 0.74 to 0.66 at average mass-flow ratios of 0.78 and 0.30, respectively, with the original nose. Shortening the nose yielded recoveries 12 to 15 percent lower than those obtained with the original nose. Shortening the nose still further and rounding the tip yielded recoveries only 5 to 7 percent less than the original values.

Total-pressure distributions at the inlet showed the presence of low-energy air at the inlet for all three nose shapes. In general, the total pressure at the inlet decreased with decreasing mass-flow ratio.

Analysis of shadowgraphs indicated unsteady flow ahead of the inlet with all three nose shapes. The flow changed from completely attached flow with a strong shock at the inlet to flow separated well upstream of the inlet and then back to attached flow, and so forth, in a manner similar to the flow oscillations associated with external compression-type inlets operating at low mass flows.

~~CONFIDENTIAL~~

INTRODUCTION



In accordance with the request of the Bureau of Aeronautics, Department of the Navy, a model simulating the inlets and forward portion of the XF3H-1 airplane has been constructed at the Langley Aeronautical Laboratory. Drag and inlet performance of this model is to be obtained in free flight over the Mach number range from about 0.8 to 1.7 by means of the rocket-model technique. Because only a limited number of pressure-survey tubes can be used in the flight test, it was necessary to calibrate these tubes by means of tests in the preflight jet at the Pilotless Aircraft Research Station at Wallops Island, Va., where more complete instrumentation was installed in the model. Although the airplane is not expected to exceed a low supersonic Mach number, the large size of the model necessitated these calibration tests at a Mach number of 1.55 in order to prevent shocks reflected from the jet boundary from intersecting the model ahead of the inlets. The results of these preflight jet tests are presented herein.

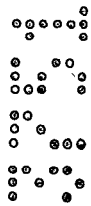
Tests were made of the original XF3H-1 configuration inlet and forebody with the original and two alternate nose shapes. Coordinates for all the configurations tested were furnished by the McDonnell Aircraft Corporation. Total-pressure profiles at the inlet, average total-pressure recoveries after 5 to 1 diffusion, and shadowgraphs of flow ahead of the inlets are presented.

In addition to the tests at Mach number 1.55, one test was made at a subsonic Mach number to check the inlet and diffuser performance in the absence of shocks on the original nose.

SYMBOLS

A	area
D	depth of inlet at a rake (see fig. 2(a))
d	distance across inlet measured from the lip inner wall (see fig. 2(a))
γ	ratio of specific heats (1.40 for air)
H	total pressure
M	Mach number

~~CONFIDENTIAL~~



\bar{m}/m_o ratio of the average mass flow through the duct to that which would flow through a free-stream tube of the same area as the inlet

p static pressure

Subscripts:

o free stream

i inlet station (21.5 in. from tip of original nose)

l inlet minimum-area station (0.2 in. downstream from inlet station)

t throat station (56.6 in. from tip of original nose)

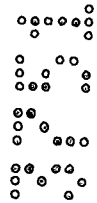
A bar (-) over a symbol represents an average value.

MODEL

A photograph and a drawing of the model are shown in figures 1(a) and 1(b), respectively. Externally, the model was a 0.147-scale version of the McDonnell XF3H-1 airplane back to the station at the rear of the pilot's canopy. Rearward of this station, transition was made from the elliptical shape of the XF3H-1 airplane forebody to a round base.

The interior contours of the inlet lips were a 0.147 scaled model of the inlet lips of the XF3H-1 airplane back to the inlet minimum-area station (A_1). The contraction ratio to this minimum-area station was 0.92, based on the total inlet area of 12.6 square inches. Figure 2(a) shows a cross-sectional view of the model at the inlet rake station, and figure 2(b) presents the lip section coordinates.

Behind the inlet minimum-area station, the model ducting differed from that of the full-scale airplane. A subsonic diffuser of about 5 to 1 area ratio was provided in order to smooth out the total-pressure profile to facilitate measurements in flight. Variation of surface area with cross-sectional area along the diffuser is shown in figure 3. After a 4-inch region of nearly constant cross-sectional area, the rate of change of diffuser surface area with cross-sectional area for the rest of the diffuser was 21.4, which value is the same as that for a 5.3° total angle conical diffuser. The data of reference 1 indicated that annular diffusers designed by this criterion had small losses when diffusing from sonic Mach number.



Transition was then made from the round diffuser exit section to a rectangular throat station with an area 1.06 times the inlet area. Figure 4 presents a cross-sectional view, at the throat station, showing the instrumentation used to measure mass flow. A duct splitter installed in the diffuser and continuing past the throat station kept the flow in the two ducts separate. Behind the throat station, the two flows were joined in a region of high velocity in order to reduce any tendency toward twin-duct instability.

Four shutters installed behind the throat regulated the air flow. They were rotated at a constant speed by an electric motor during the tests. The rate of air-flow variation was such as to go from maximum mass flow to minimum mass flow in approximately 13 seconds. This shutter speed was used since it was found in tests of a previous model (reference 2) to be slow enough to yield the same results as did tests with fixed shutters. The duct downstream of the shutters made a transition to a round area of 1.6 times the inlet area and was cylindrical to the exit.

Three different nose shapes were tested. The coordinates used for these three nose shapes, scaled down from the coordinates supplied by the McDonnell Aircraft Corporation, are shown in figure 5. The first was the nose shape of the XF3H-1 airplane and is referred to as nose A. The second (nose B), somewhat similar to nose A, was shorter and had a larger apex angle. The third nose (nose C) was shorter than the second and was initially round.

The nose, inner body, inlet lips, duct splitter, and all internal ducting for the model were made of magnesium. The canopy, wheel well, and all of the model exterior back of the inlet lips were made of mahogany.

INSTRUMENTATION

Total pressure at the right-inlet minimum-area station was measured with twelve 0.09-inch outside-diameter total-pressure tubes flattened at the forward end. As shown in figure 2(a), they were arranged in three rakes of four tubes each. Static pressure was measured at the same station with an inner-body wall orifice. Two total-pressure tubes and one static-pressure orifice, located at the same station (as shown in fig. 2(a)), were used in the left inlet duct.

Twenty 0.09-inch outside-diameter total-pressure tubes were installed in the left duct at the throat station (as shown in fig. 4). Static pressure at the same station in each duct was measured by two wall orifices manifolded together. In addition, the left duct had two static-pressure probes located on the rake (as shown in fig. 4).

o o o o o
o o o o o
o o o o o
o o o o o
o o o o o

The free-stream total pressure, static pressure at the jet nozzle exit, and total pressure at the tip of each nose were also measured. Pressures were recorded by mechanical optical pressure recorders and electrical pressure recorders of the strain-gage type. Time histories were obtained on film. Shadowgraphs were taken of all tests.

TESTS

The tests were made in the preflight jet at the Pilotless Aircraft Research Station, Wallops Island, Va. (reference 3). A 27-inch square, Mach number 1.55 nozzle was used. Tests were not conducted at a lower supersonic Mach number because, at $M < 1.55$, shock reflections from the jet boundaries would intersect the model ahead of the inlets.

Each test was started with the air-flow-regulation shutters in position to give maximum mass flow. The test was continued until the shutters had rotated to such a position as to give minimum mass flow. The model throughout all tests was at 0° angle of attack and 0° angle of yaw. The Reynolds number for all supersonic tests was approximately 11 million per foot.

A subsonic test at $M_0 \approx 0.7$ was also made with the supersonic nozzle. This Mach number was obtained by decreasing the reservoir total pressure to a point where the normal shock moved back inside the nozzle and upstream of the most forward point of the model. A static-pressure survey along the nozzle was used to determine the position of the normal shock. The total pressure measured by the tube located in the tip of the model nose was used as free-stream stagnation pressure. The Reynolds number for this subsonic test was approximately 3 million per foot.

ANALYSIS

At a Mach number of 1.55, all pressure measurements made at the inlet and throat exhibited approximately 60-cycle oscillations with an amplitude of about 5 percent of the full-scale displacement. Since the instrumentation employed made instantaneous measurements inaccurate, the midpoint of the oscillation was used as the average pressure at any given time. Hereinafter, it will be understood that all values of pressures referred to were obtained in this manner.

Since the total-pressure profile at the throat station was essentially flat, within 1 percent of the average, the numerical average of the 20-tube readings was taken as the average total pressure \bar{H}_t . The three static-



pressure measurements in the left duct agreed within 2 percent of each other, and the numerical average was used as the static pressure \bar{p}_t . The average Mach number at the throat \bar{M}_t was then obtained from the ratio of \bar{p}_t and \bar{H}_t . The average mass-flow ratio was calculated according to the following equation:

$$\frac{\bar{m}}{\bar{m}_0} = \frac{\bar{p}_t A_t \bar{M}_t \left(1 + \frac{\gamma - 1}{2} \bar{M}_t^2\right)^{1/2}}{p_0 A_i M_0 \left(1 + \frac{\gamma - 1}{2} M_0^2\right)^{1/2}}$$

RESULTS AND DISCUSSION

The total-pressure recovery after diffusion is plotted in figure 6 against mass-flow ratio for the three nose shapes tested. The recovery obtained with nose A was a maximum (0.74) at the maximum mass-flow ratio attained (0.78). Maximum mass-flow ratio was limited in these tests by choking at the rake supports aft of the throat station where the presence of the tubes and the rake supports reduced the left duct area to 84 percent of the left inlet area and reduced the right duct area to 94 percent of the right inlet area. The recovery decreased with decreasing mass flow to a minimum value of about 0.66 which was obtained over a range of mass-flow ratios from 0.3 to 0.6. Thus, with the original nose shape, the total-pressure recovery after diffusion was from 19 to 28 percent lower than the normal shock recovery at the free-stream Mach number. Both nose B and nose C yielded lower total-pressure recoveries than nose A. The recovery with nose B ranged from 0.58 at $\frac{\bar{m}}{\bar{m}_0} = 0.6$ to 0.55 at $\frac{\bar{m}}{\bar{m}_0} = 0.2$, while, with nose C, the recovery had a relatively constant value of about 0.63.

Figure 7 presents the total-pressure profiles measured at the inlet with nose A for three different mass-flow ratios at $M_0 = 1.55$, and for one mass-flow ratio at $M_0 \approx 0.7$. The mass-flow ratios and total-pressure recoveries after diffusion, shown for reference, were determined from throat measurements in the left duct. The profile shapes show the presence of boundary layer of considerable depth entering the inlet. It can also be seen that generally the total pressure at the inlet decreased with decreasing mass flow and, although it would be impossible to determine an accurate value of average total pressure at the inlet from these profiles, they do indicate that a large percentage of the losses measured

after diffusion occurred prior to the inlet and were not just a result of large subsonic diffuser losses.

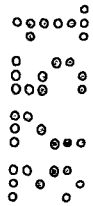
The flagged symbols show the two total pressures measured in the left inlet and the dashed line shows the static pressure measured in the left inlet. The two total-pressure measurements in the left inlet show only fair agreement with the center rake survey in the right inlet, but the static pressures obtained on each side are in good agreement.

The inlet total-pressure profile presented at the extreme right of figure 7 was measured during the subsonic test at $M_0 \approx 0.7$. The three rakes give almost identical profiles, leading to the conclusion that the subsonic flow at the inlet is reasonably uniform. The recovery at the inlet was 0.97, while the recovery after diffusion was 0.94, indicating again that the low recovery measured at $M_0 = 1.55$ was not a result of large diffuser losses.

The total-pressure profiles at the inlet for nose B are shown in figure 8. In the profiles shown for mass-flow ratios of 0.60 and 0.46, the rake at the top near the pilot's canopy showed a separated flow region with extremely low recovery while, at $\frac{\bar{m}}{m_0} = 0.25$, a low recovery region was recorded by the middle rake. As the flagged symbols indicate, the measurements made in the left inlet showed good agreement at the higher mass-flow ratios while, at the low mass-flow ratios, they agree only in that they show a region of low recovery and probable separation.

Figure 9 shows the total-pressure profiles measured at the inlet with nose C for three mass-flow ratios. At a mass-flow ratio of 0.67, the distribution obtained from the top rake near the pilot's canopy shows separation near the inner wall. The other two rakes indicate a relatively thick boundary layer at the inlet. At $\frac{\bar{m}}{m_0} = 0.55$, the top rake no longer shows separated flow, while at $\frac{\bar{m}}{m_0} = 0.20$, the recovery recorded by the top rake is the highest of the three rakes. The other rakes show decreasing recovery as mass flow decreases. With this nose shape, the pressure measurements made in the left inlet show good agreement with the center rake survey in the right inlet.

Figure 10 presents a series of shadowgraphs with nose A as viewed from the top, taken consecutively at 0.5-second intervals. The right inlet appears at the top of the picture and the flow is from left to right. Shocks from the canopy and wheel well are seen at the left of all pictures and do not change appreciably with \bar{m}/m_0 .



Although the shadowgraphs show nearly instantaneous flow conditions (exposure time about 5 microseconds) the 0.5-second interval between pictures does not allow any conclusions to be drawn regarding the frequency and extent of the shock cycles. The values of mass-flow ratio and total-pressure recovery given for each picture are the average values as discussed in the section entitled "Analysis."

Figures 10(a) to 10(d) show the shock configuration at the maximum mass-flow ratio of 0.79 and pressure recovery of 0.74 obtained with nose A. Because of choking at the tube supports behind the throat, the shutters were ineffective in changing the mass-flow ratio during that part of the test.

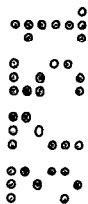
The shadowgraphs show that the shock pattern ahead of the right inlet changed only slightly. Ahead of the left inlet, however, the lambda foreleg moved forward (as seen in figs. 10(b) and 10(c)), and separation apparently took place aft of this lambda leg. The separated flow seems to be entering the inlet. In figure 10(d), the shock pattern has become similar to that of the first shadowgraph (fig. 10(a)).

Beginning with figure 10(e), the mass-flow ratio varied while the rest of the pictures were taken. As the sequence shows, the flow ahead of the inlets is unsteady, varying from picture to picture in a manner which cannot be correlated on the basis of mass-flow ratio alone.

The flow variation goes from that with a strong shock at the inlet in figure 10(g) to that with complete separation far forward on the body (fig. 10(j)) and subsonic flow to the inlet. The same variation in successive frames can be seen in figures 10(l), 10(m), and 10(n). At this lower mass-flow ratio, however, the separated flow ahead of the inlet, seen in figure 10(m), appears to be completely subsonic, whereas in the next frame the flow has again reattached and the strong shock is again at the inlet. The same type of flow oscillations occurred with the other two noses, and sample shadowgraphs are shown in figures 11 and 12 for noses B and C, respectively.

The pressure oscillations that occurred during the tests of all three noses apparently resulted from this shock movement. This flow phenomenon appears to be similar to the unsteady flow characteristics of an external compression inlet operating at low mass-flow ratios.

Results similar to these have been obtained by a previous investigation reported in reference 4. Model D of reference 4 was quite similar to that of this report, except it was a sharp-lip annular inlet with no canopy or wheel well. Low recoveries after diffusion and flow unsteadiness at mass-flow ratios less than maximum are reported throughout the Mach number range tested, 1.36 to 2.01.



CONCLUSIONS

Free-jet tests were made of a model of the McDonnell XF3H-1 airplane forebody and inlets at a Mach number of 1.55 and 0° angle of attack and yaw. At this Mach number, the pressure measurements made at the inlet and after diffusion showed high frequency oscillations, generally sinusoidal in appearance. The results of these tests, based on the average of the oscillatory pressures, indicated the following:

- (1) The total-pressure recovery after 5 to 1 diffusion with the original pointed nose ranged from 0.74 to 0.66 at mass-flow ratios of 0.73 and 0.30, respectively.
- (2) A shortened pointed nose shape yielded recoveries from 12 to 15 percent lower than those obtained with the original nose.
- (3) Shortening the nose still further and rounding the tip yielded recoveries only 5 to 7 percent less than the values obtained with the original nose.
- (4) Total-pressure profiles taken at the inlet showed the presence of low-energy air in the inlet with total pressure decreasing with decreasing mass flow for all three nose shapes.
- (5) Analysis of shadowgraph pictures indicated unsteady flow ahead of the inlet throughout the mass-flow range tested for all three nose shapes, similar to the unsteady flow phenomenon associated with external compression inlets.

Langley Aeronautical Laboratory
National Advisory Committee for Aeronautics
Langley Field, Va.

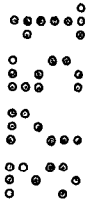
Charles F. Merlet
Aeronautical Research Scientist

Howard S. Carter
Aeronautical Research Scientist

Approved:

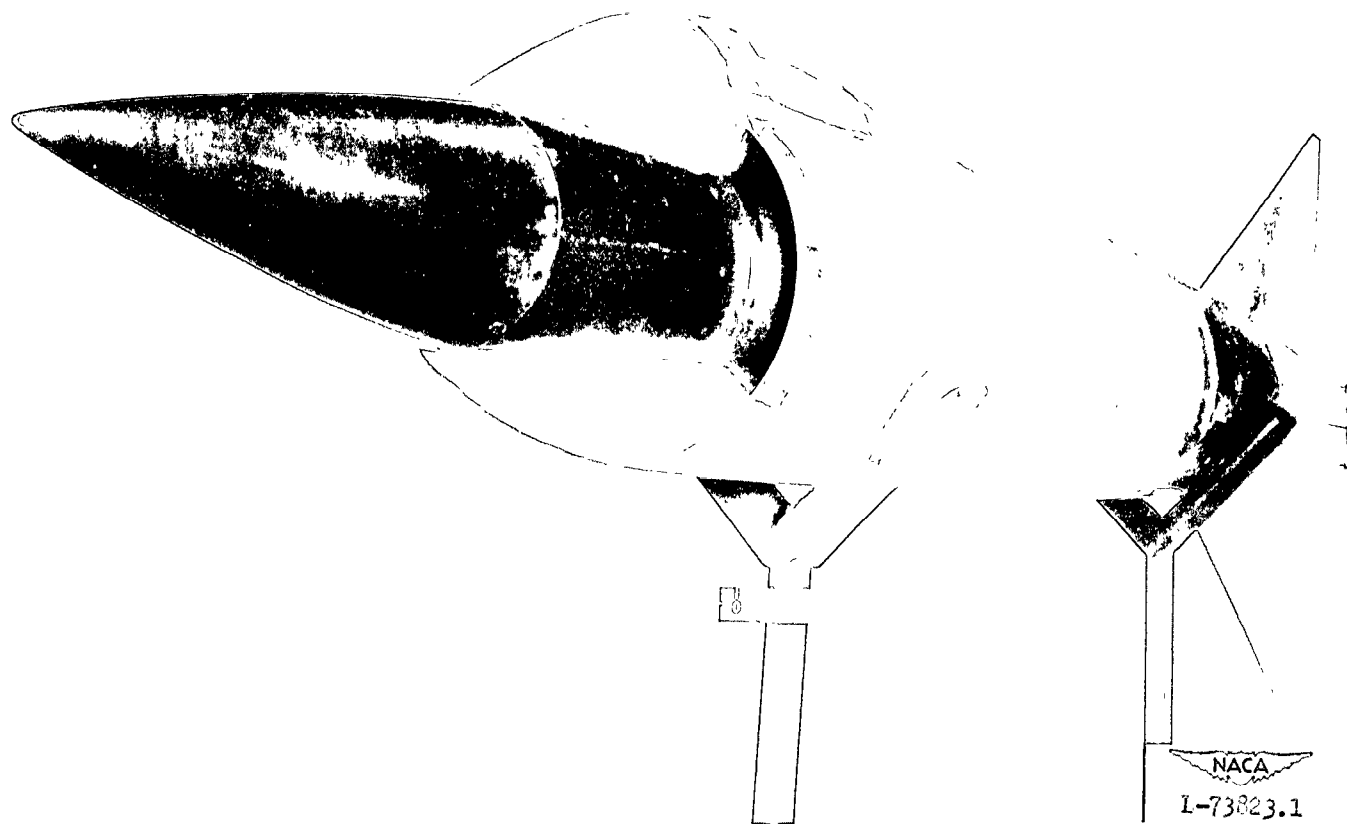
Joseph A. Shortal
Chief of Pilotless Aircraft Research Division

JLC



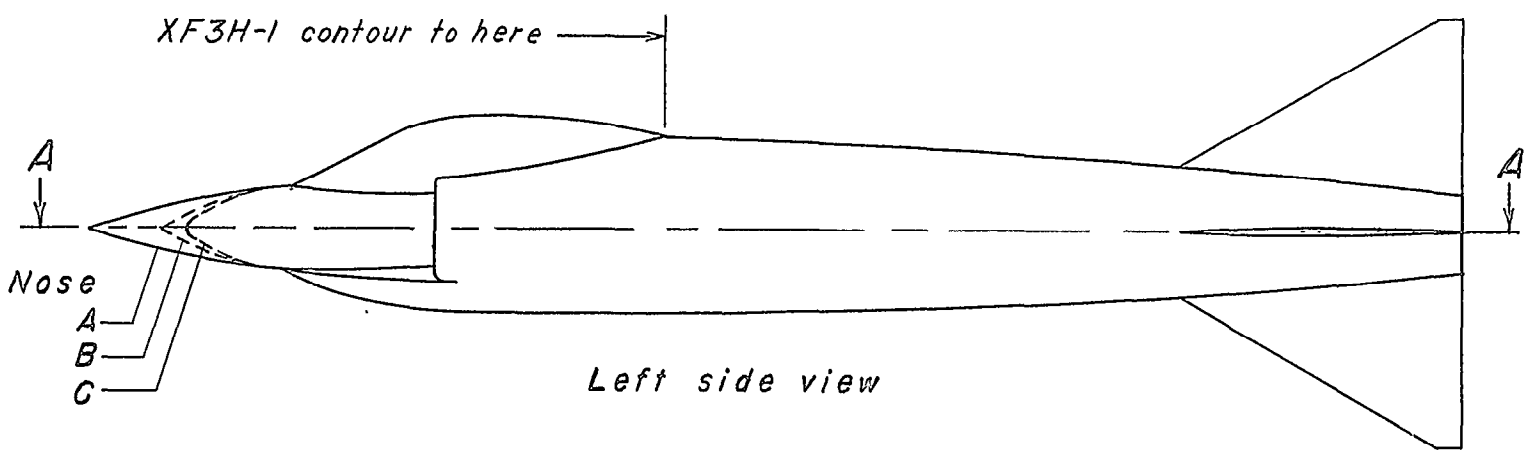
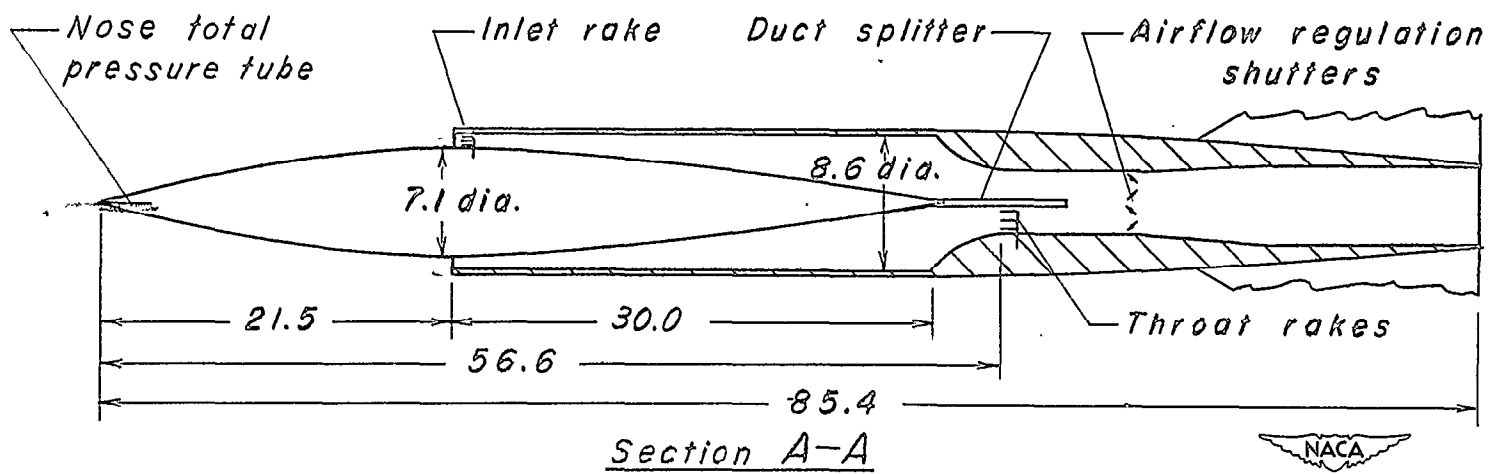
REFERENCES

1. Bohm, H., and Koppe, M.: The Influence of Friction on Steady Diffuser Flows at High Speed. B.I.G.S. - 47, Joint Intelligence Objectives Agency, Washington, D. C., July 23, 1946.
2. Merlet, Charles F., and Carter, Howard S.: Total-Pressure Recovery of a Circular Underslung Inlet with Three Different Nose Shapes at a Mach Number of 1.42. NACA RM L51K05, 1951.
3. Faget, Maxime A., Watson, Raymond S., and Bartlett, Walter A., Jr.: Free-Jet Tests of a 6.5-Inch Diameter Ram-Jet Engine at Mach Numbers of 1.81 and 2.00. NACA RM L50L06, 1951.
4. Davis, Wallace F., Brajnikoff, George B., Goldstein, David L., and Spiegel, Joseph M.: An Experimental Investigation at Supersonic Speeds of Annular Duct Inlets Situated in a Region of Appreciable Boundary Layer. NACA RM A7G15, 1947.



(a) Photograph of the model.

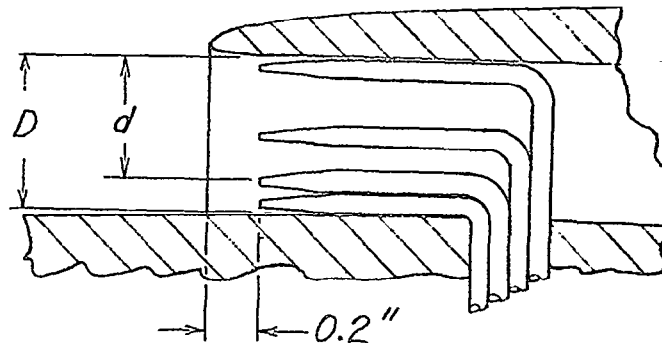
Figure 1.- General arrangement of the model.



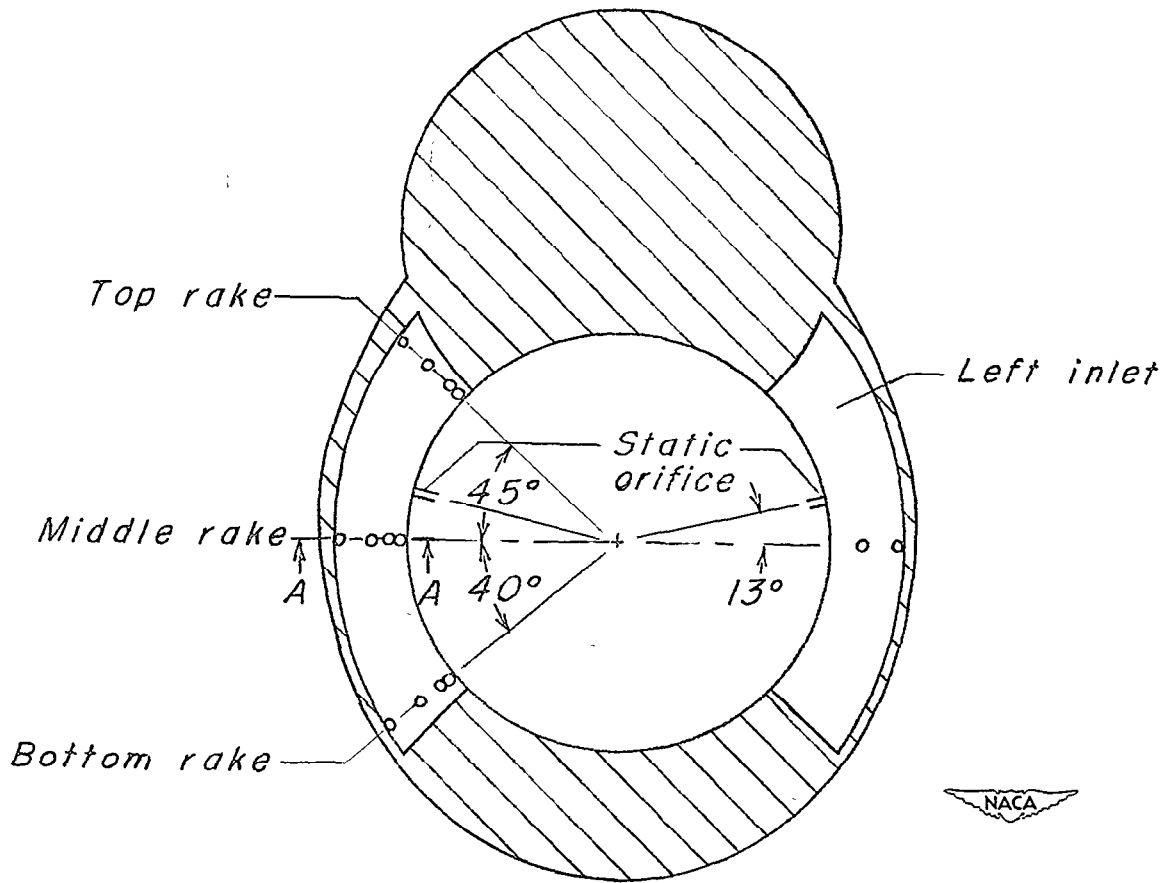
(b) Drawing of the model. All dimensions are in inches.

~~CONFIDENTIAL~~

100
100
100
100
100
100
100



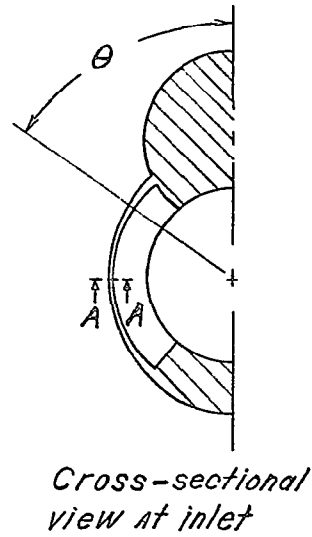
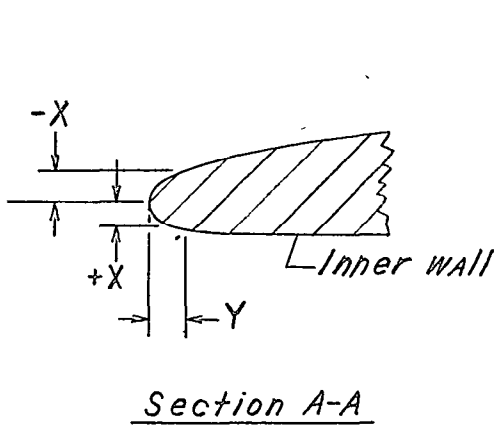
- Section A-A
(Typical rake)



(a) Cross-sectional view at the inlet minimum-area station, showing instrumentation.

Figure 2.- Details of the inlet.

~~CONFIDENTIAL~~



Lip section coordinates										
Y	$\theta = 40^\circ$		$\theta = 60^\circ$		$\theta = 90^\circ$		$\theta = 115^\circ$		$\theta = 135^\circ$	
	+X	-X	+X	-X	+X	-X	+X	-X	+X	-X
0.015	0.026	0.035	0.024	0.028	0.022	0.026	0.024	0.029	0.031	0.035
.029	.034	.050	.031	.043	.029	.038	.031	.044	.038	.050
.074	.049	.082	.046	.065	.043	.059	.046	.068	.056	.085
.118	.056	.103	.054	.082	.050	.074	.054	.084	.065	.107
.176	.059	.126	.056	.101	.051	.088	.056	.103	.066	.131
.294		.162		.129		.113		.134		.166
.441		.190		.153		.135		.157		.196
.588		.215		.173		.153		.176		.222
.882		.248		.200		.178		.204		.257
1.176		.269		.218		.194		.222		.279



(b) Lip-section coordinates. All dimensions are in inches.
Figure 2.- Concluded.

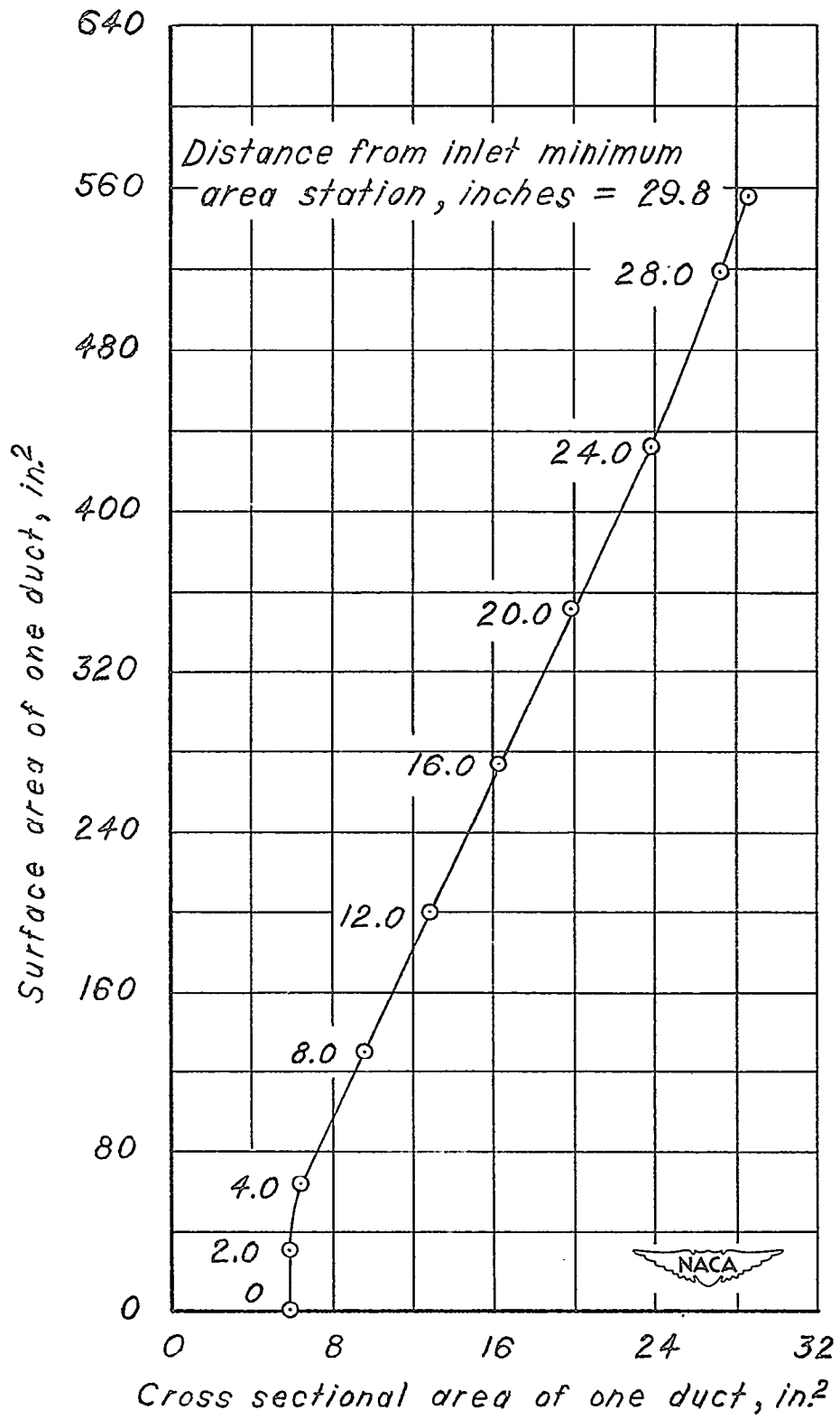
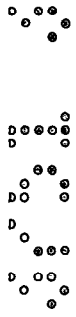
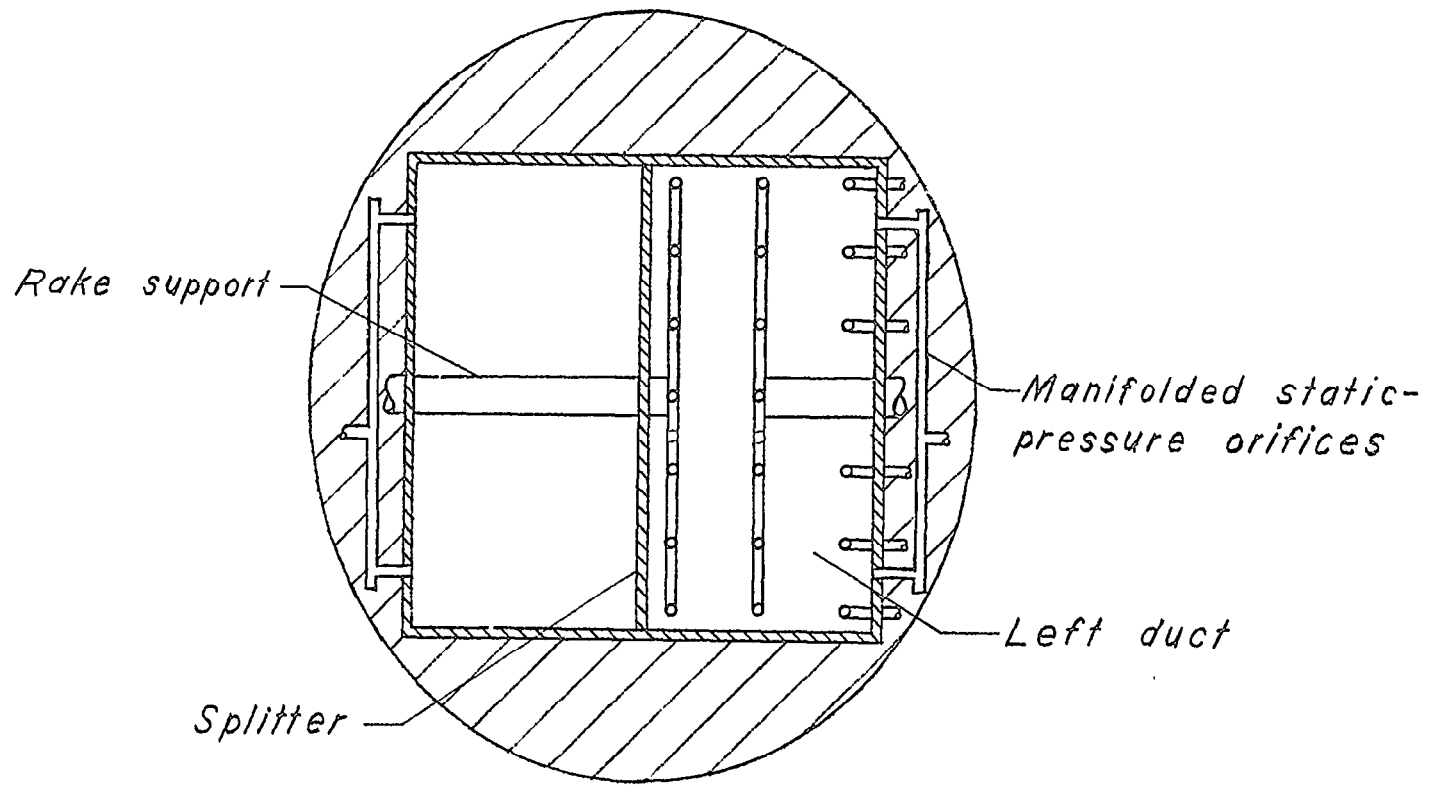
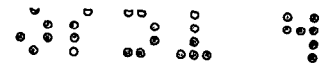


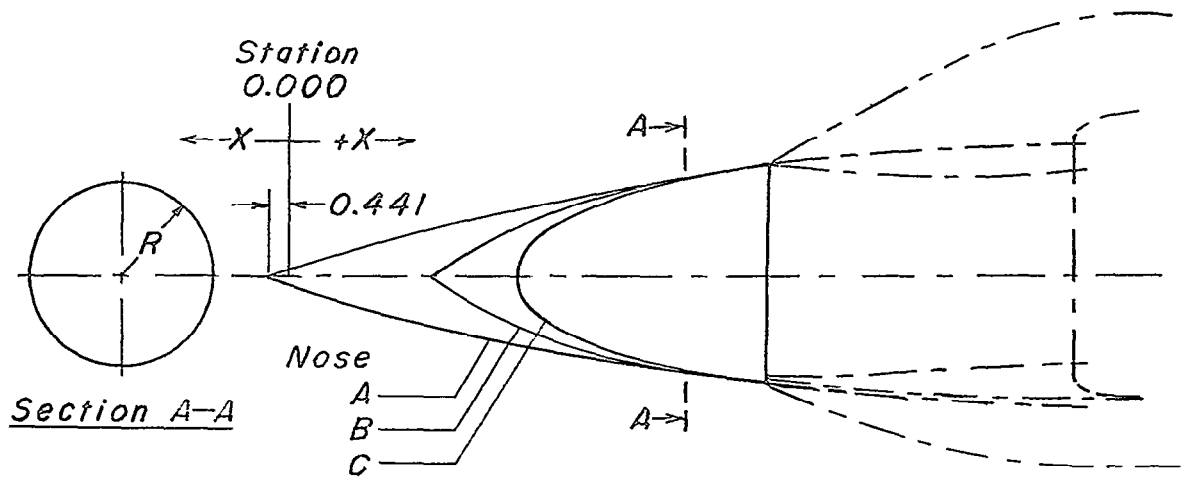
Figure 3.- Variation of diffuser surface area with cross-sectional area.



- o Total-pressure tube
- o Static-pressure tube



Figure 4.- Cross-sectional view at the throat station, showing instrumentation.



Nose A		Nose B		Nose C	
X	R	X	R	X	R
-0.441	0.000	4.292	0.000	5.439	0.000
-0.110	0.104	4.704	0.332	5.585	0.538
1.029	0.448	5.439	0.859	5.880	0.905
2.499	0.866	6.174	1.298	6.321	1.244
3.969	1.250	6.909	1.654	6.909	1.558
5.439	1.602	7.644	1.938	7.644	1.851
6.909	1.924	8.379	2.161	8.379	2.082
8.379	2.215	9.114	2.337	9.114	2.272
9.849	2.475	9.849	2.476	9.849	2.434
12.642	2.889	11.319	2.706	11.319	2.699
		12.642	2.889	12.642	2.889



Figure 5.- Coordinates of the three noses. All dimensions are in inches.

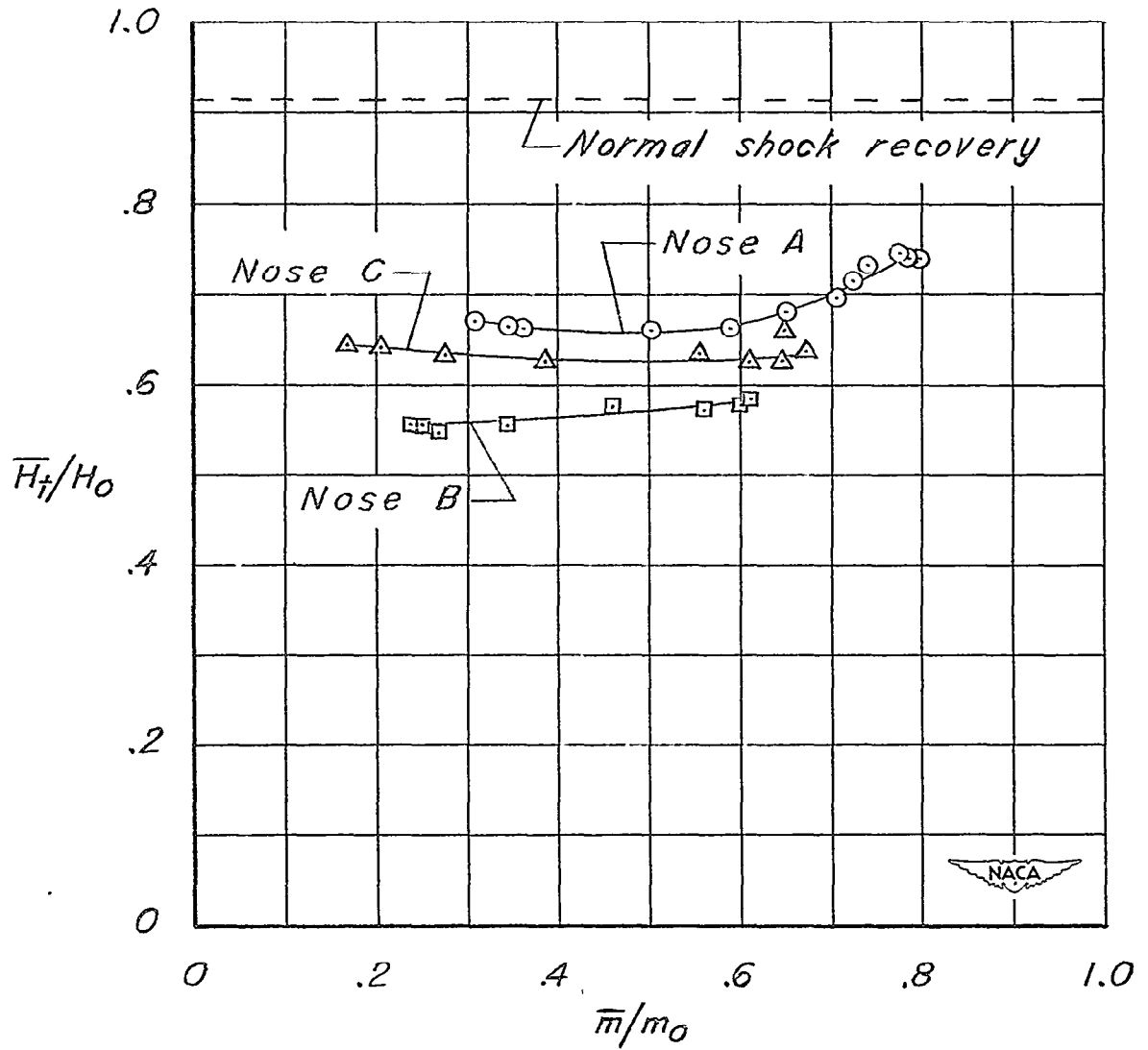


Figure 6.- Total-pressure recovery after diffusion as a function of mass-flow ratio for the three noses. $M_0 = 1.55$.

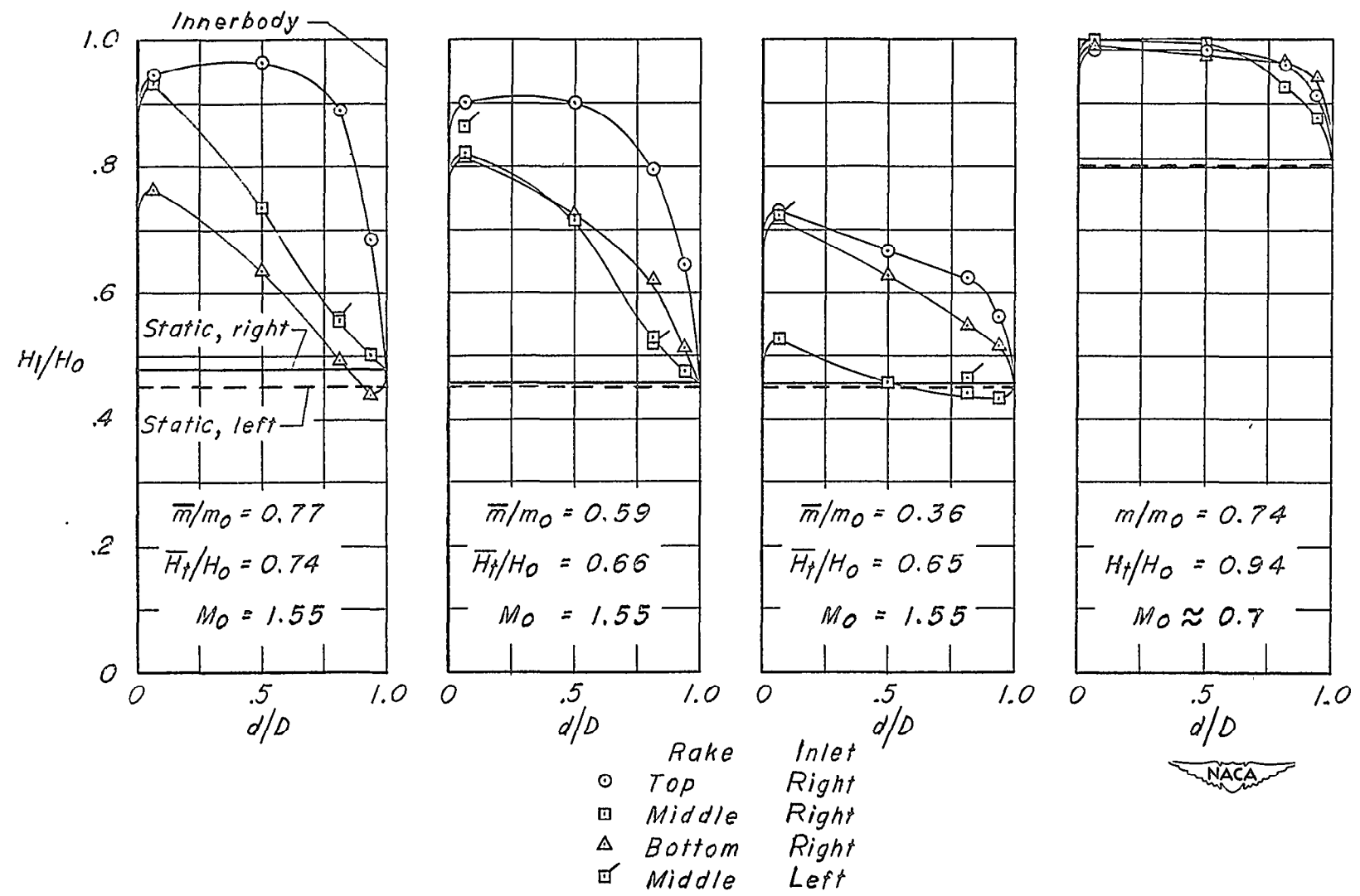


Figure 7.- Total-pressure-recovery profiles at the inlet minimum-area station with nose A.



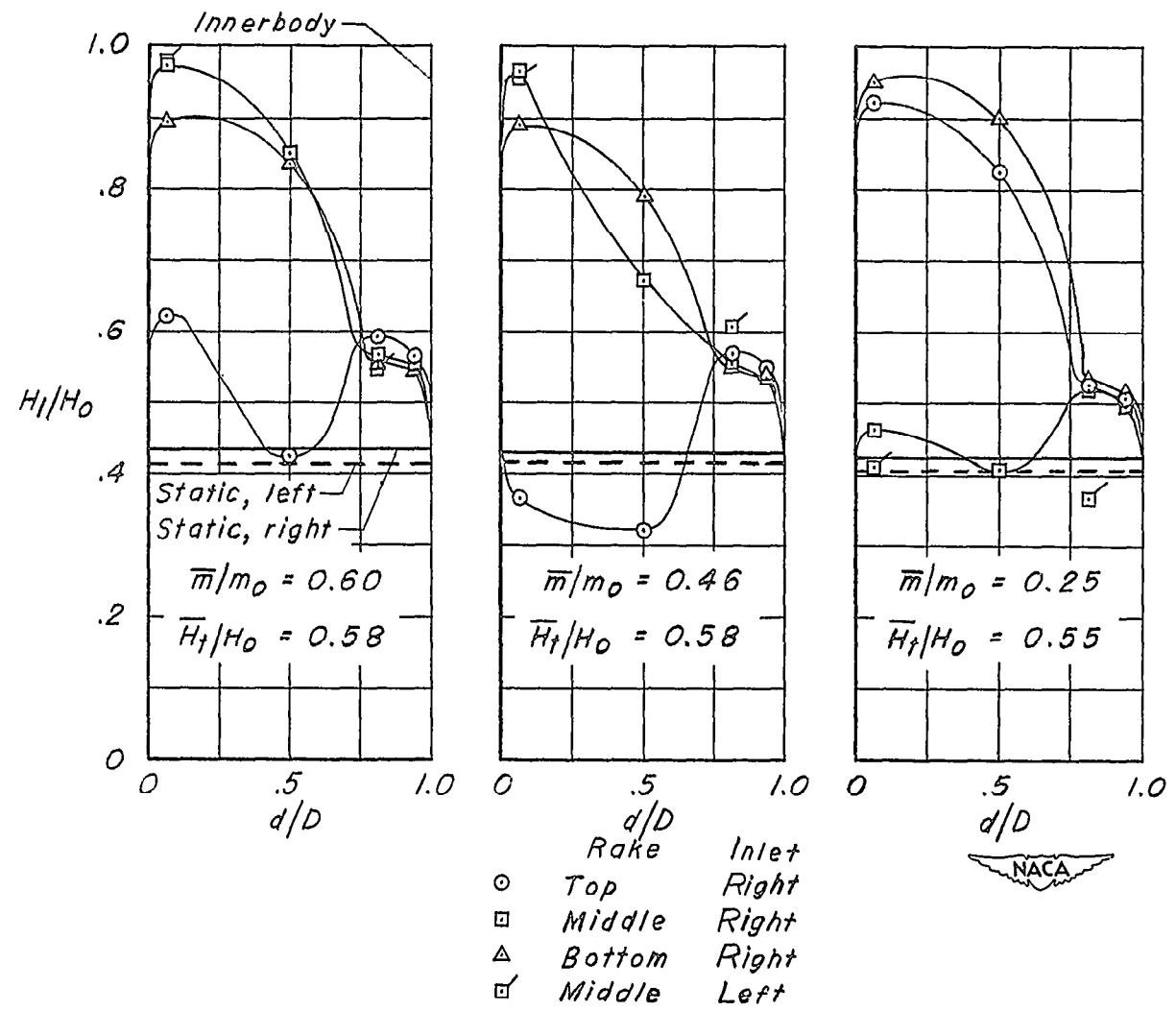
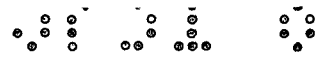


Figure 8.- Total-pressure-recovery profiles at the inlet minimum-area station with nose B. $M_0 = 1.55$.

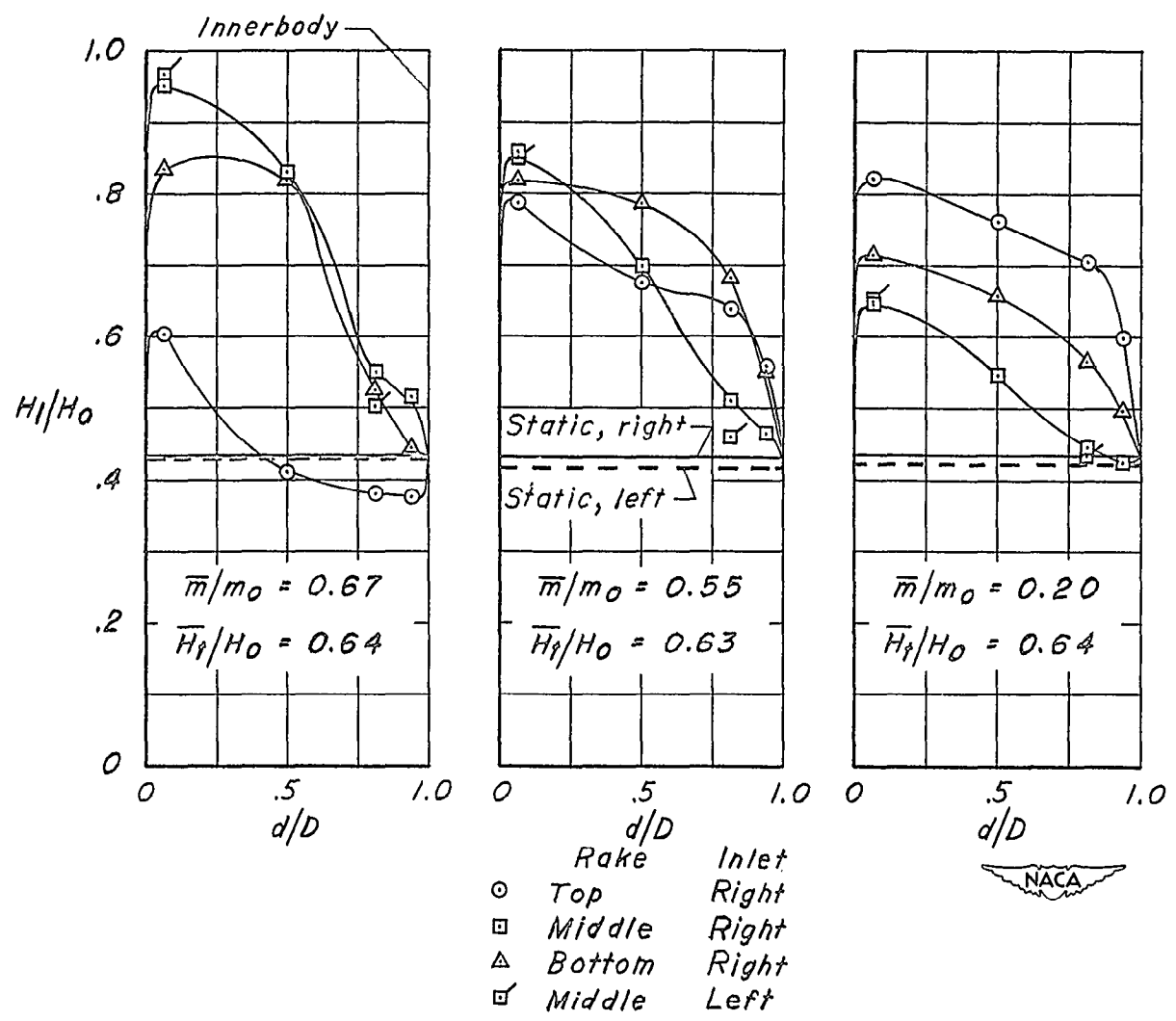


Figure 9.- Total-pressure-recovery profiles at the inlet minimum-area station with nose C. $M_0 = 1.55$.



(a) $\frac{\bar{m}}{m_0} = 0.79$; $\frac{\bar{H}_t}{H_0} = 0.74$; time, 0 second.

NACA
L-74334

Figure 10.- Shadowgraphs showing unsteady flow at various average mass-flow ratios and total-pressure recoveries. Nose A; $M_0 = 1.55$.

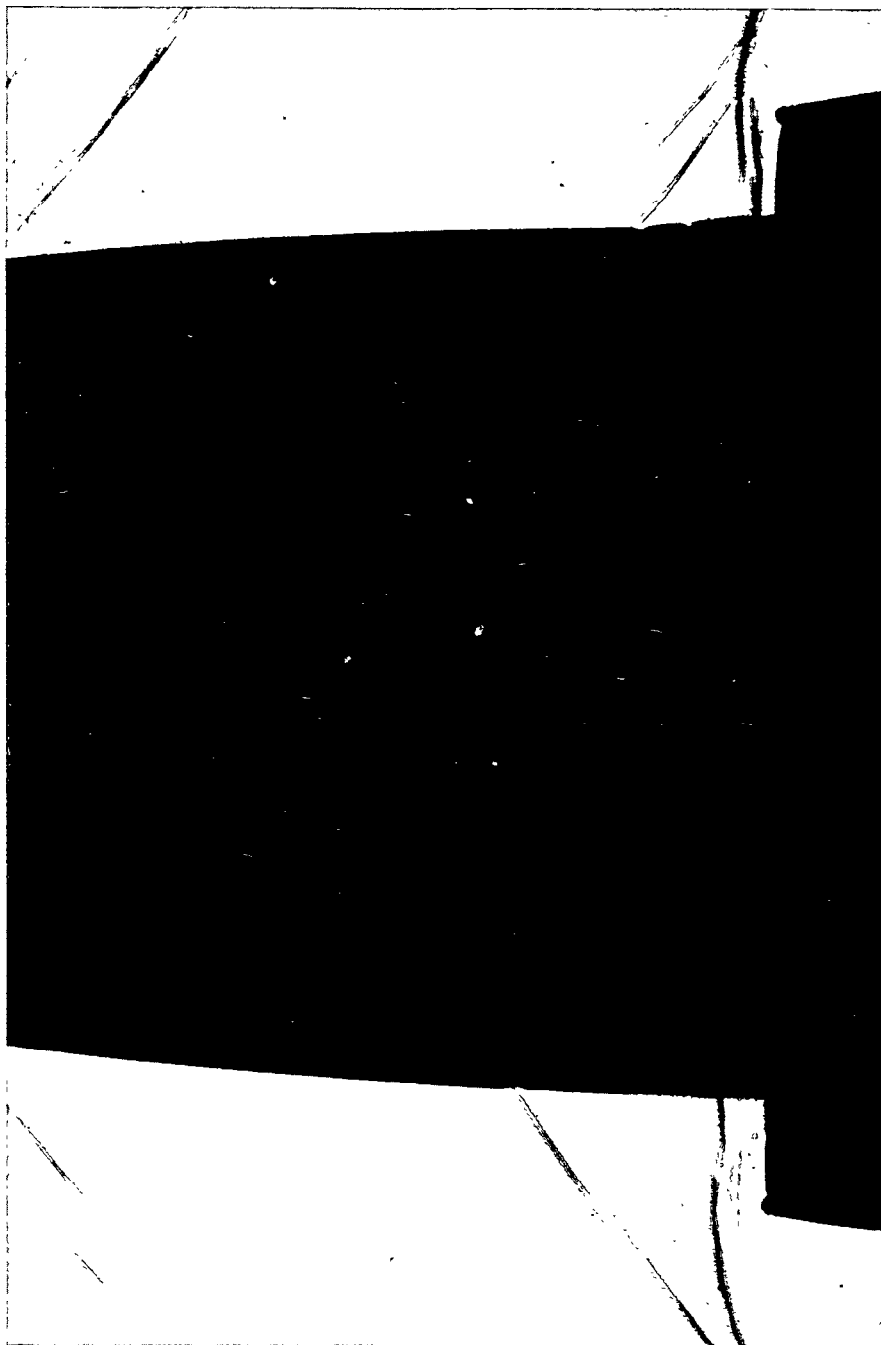


(b) $\frac{\bar{m}}{m_0} = 0.79$; $\frac{\bar{H}_t}{H_0} = 0.74$; time, 0.5 second.

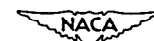


L-74335

Figure 10.- Continued.

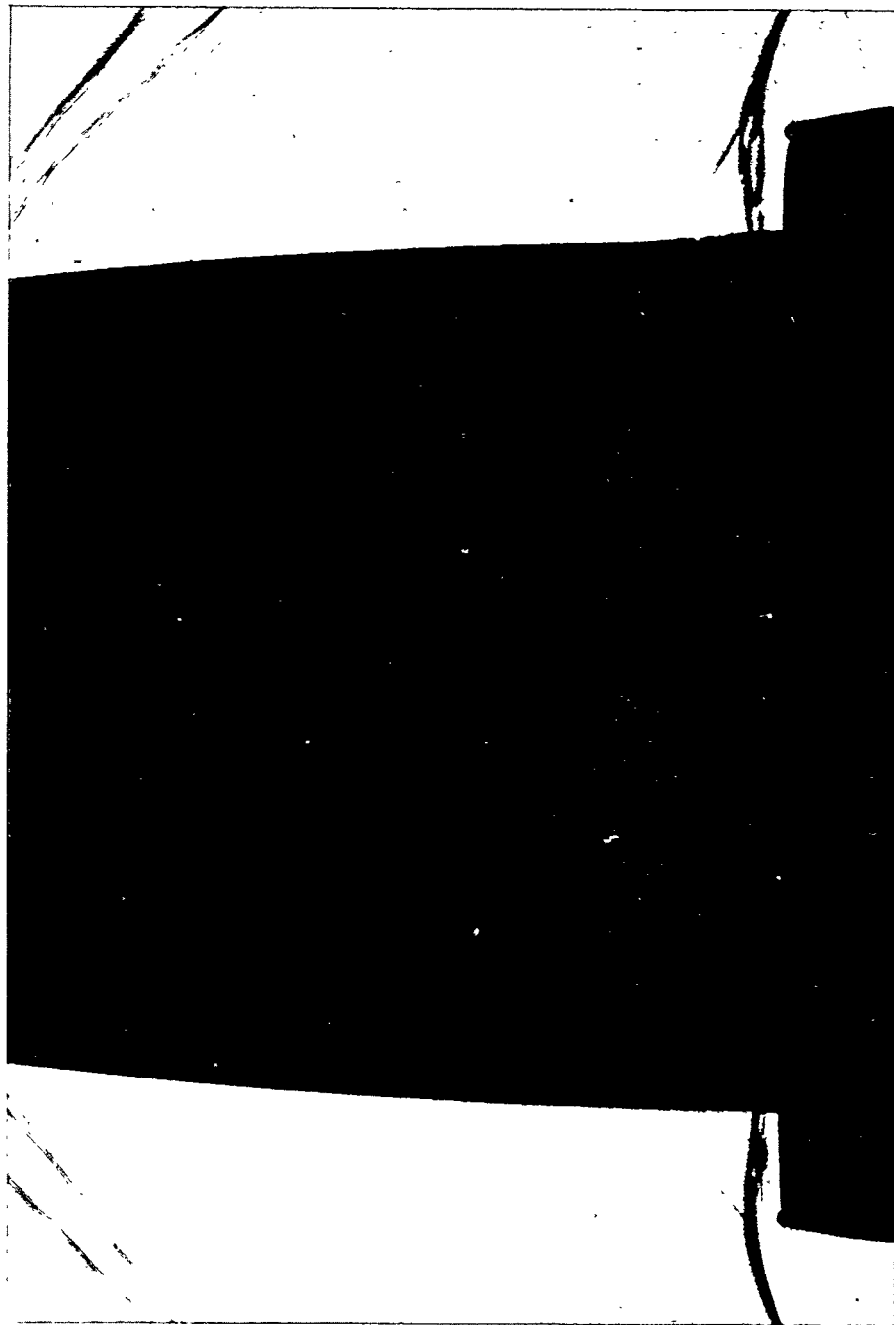


(c) $\frac{\bar{m}}{m_0} = 0.79$; $\frac{\bar{H}_t}{H_0} = 0.74$; time, 1.0 second.



L-74336

Figure 10.- Continued.



(d) $\frac{\bar{m}}{m_0} = 0.79$; $\frac{\bar{H}_t}{H_0} = 0.74$; time, 1.5 seconds.



L-74337

Figure 10.- Continued.

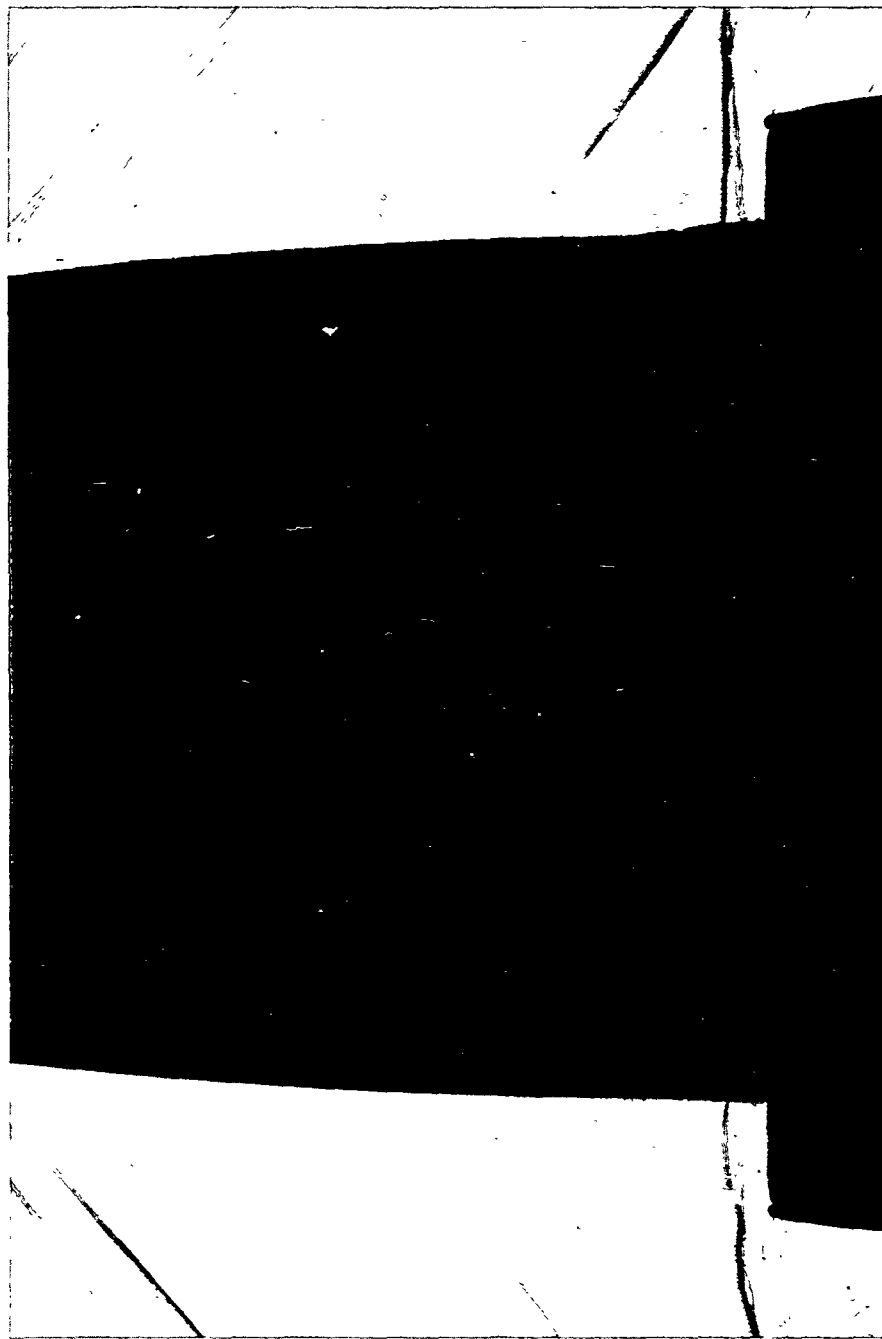


(e) $\frac{\bar{m}}{m_0} = 0.77$; $\frac{\bar{H}_t}{H_0} = 0.73$; time, 2.0 seconds.



L-74338

Figure 10.- Continued.

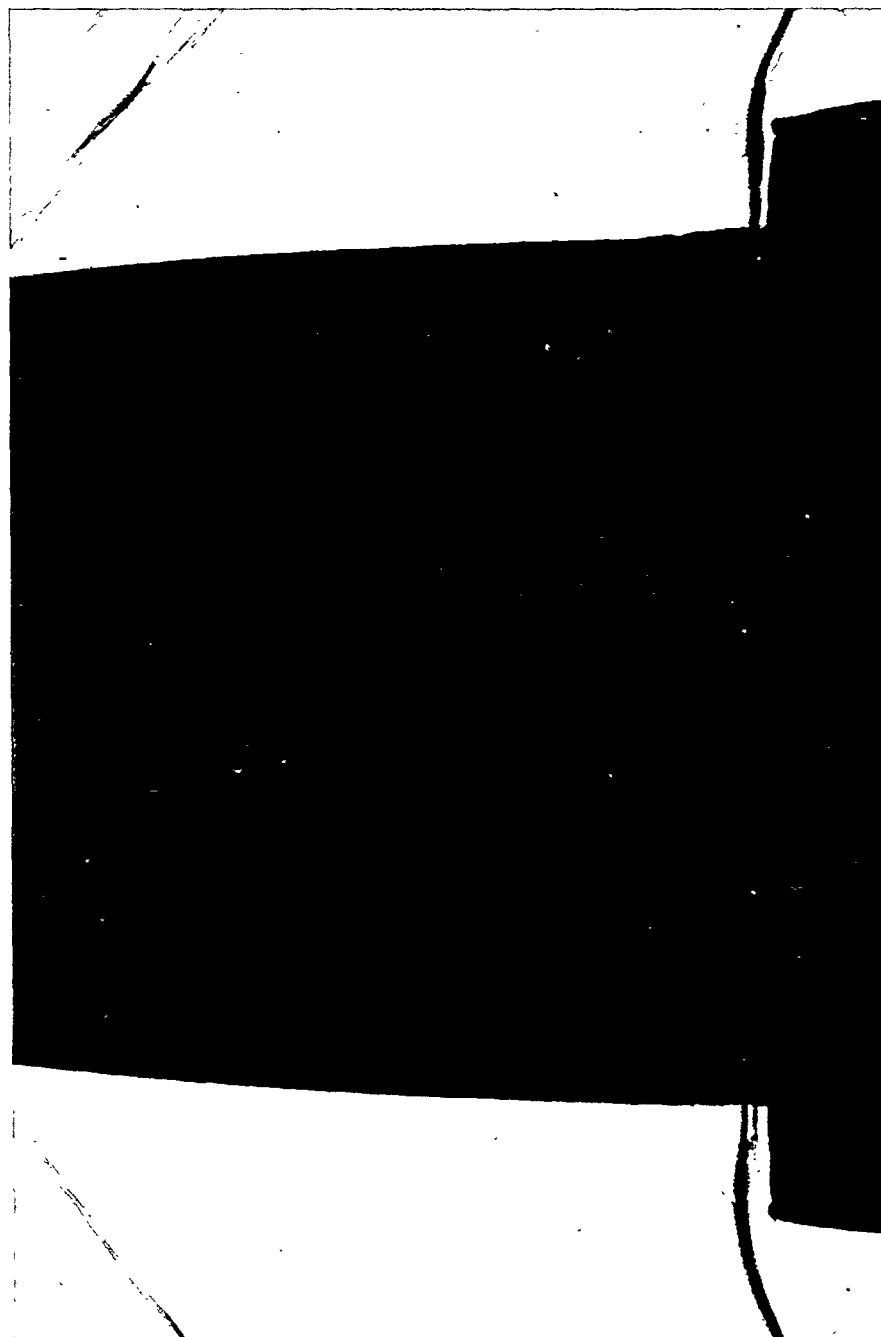


(f) $\frac{\bar{m}}{m_0} = 0.75$; $\frac{\bar{H}_t}{H_0} = 0.72$; time, 2.5 seconds.



L-74339

Figure 10.- Continued.

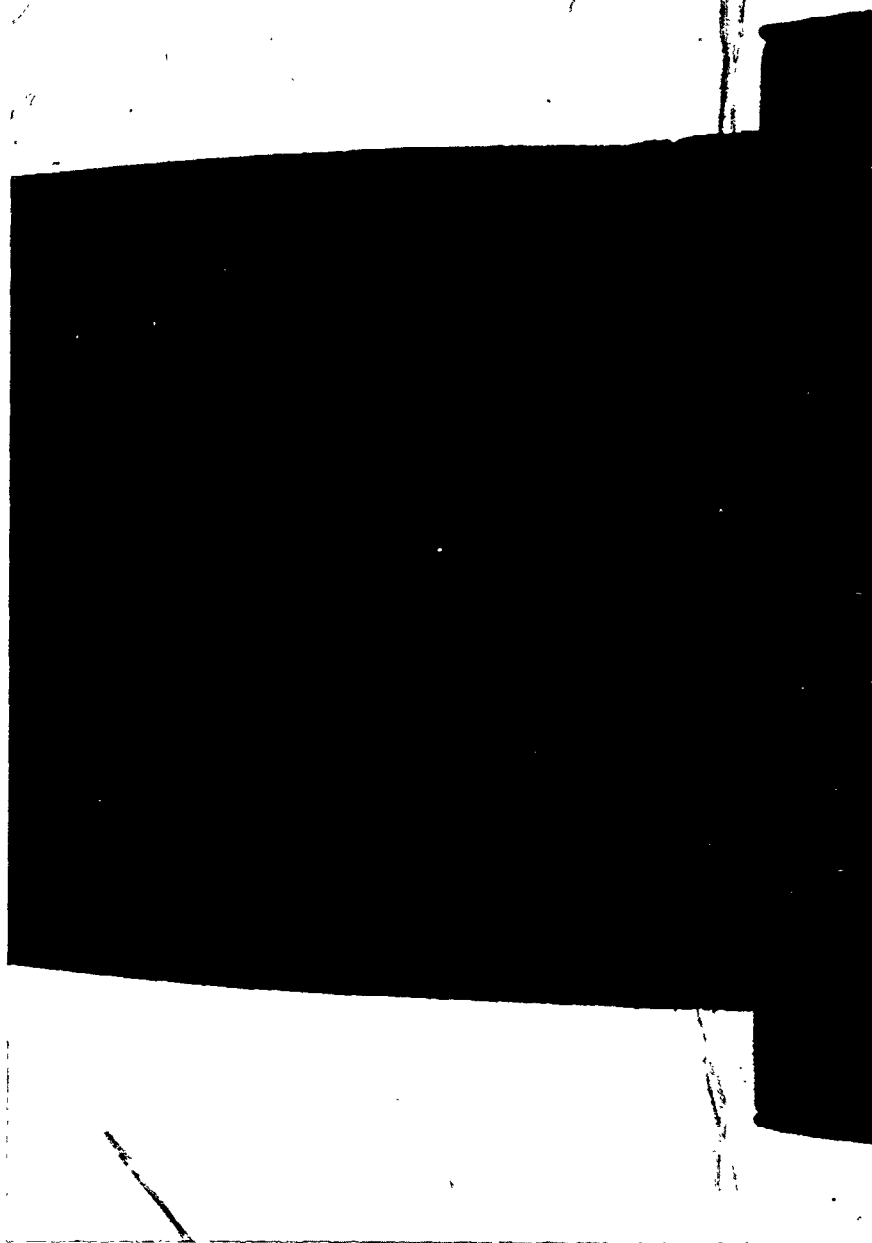


(g) $\frac{\bar{m}}{m_0} = 0.73$; $\frac{\bar{H}_t}{H_0} = 0.71$; time, 3.0 seconds.

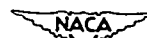


L-74340

Figure 10.- Continued.

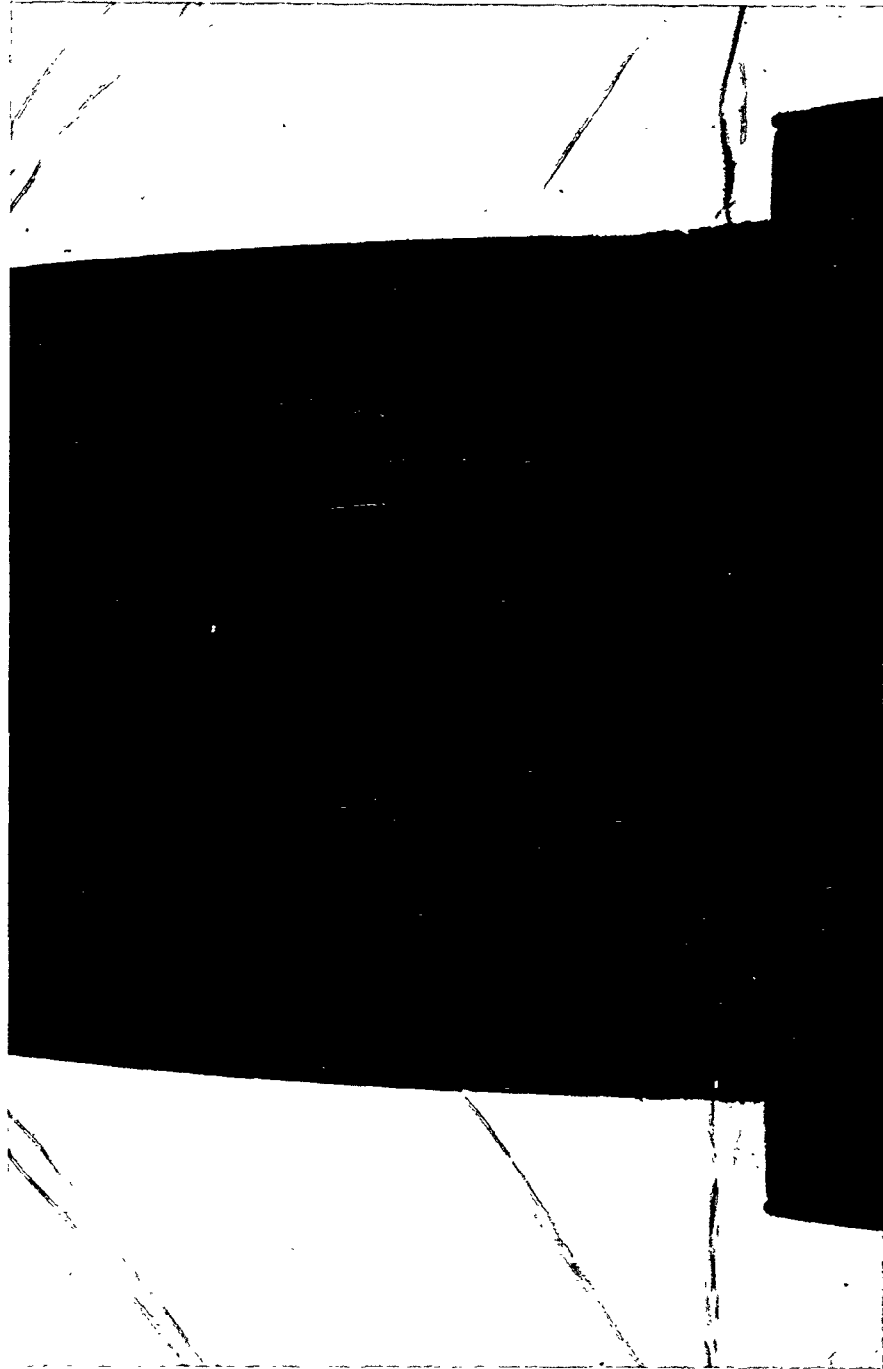


(h) $\frac{\bar{m}}{m_0} = 0.69$; $\frac{\bar{H}_t}{H_0} = 0.69$; time, 3.5 seconds.



L-74341

Figure 10.- Continued.



(i) $\frac{M}{M_0} = 0.64$; $\frac{H_t}{H_0} = 0.67$; time, 4.0 seconds.



L-74342

Figure 10.- Continued.



(j) $\frac{\bar{m}}{m_0} = 0.61$; $\frac{\bar{H}_t}{H_0} = 0.66$; time, 4.5 seconds.



L-74343

Figure 10.- Continued.



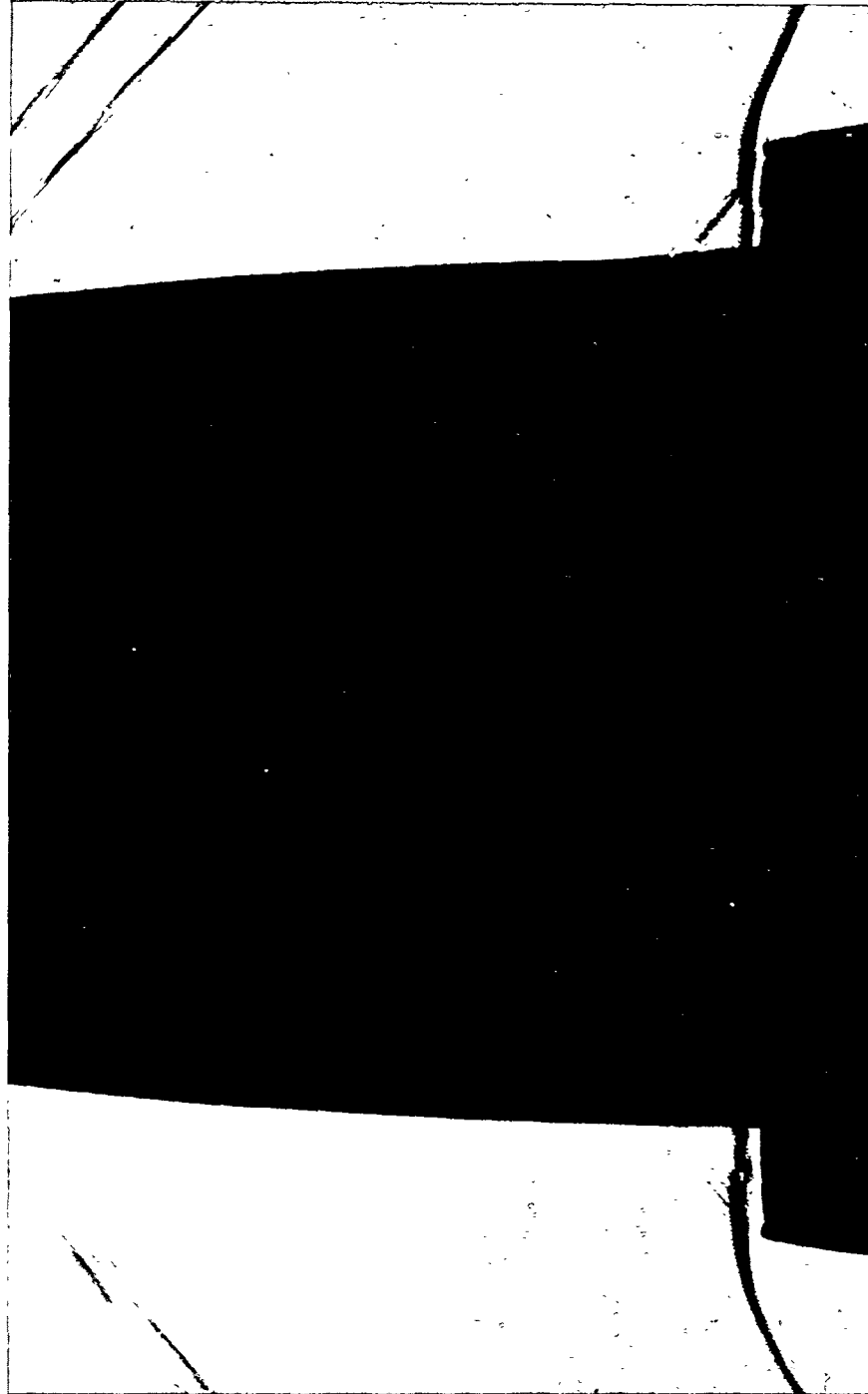
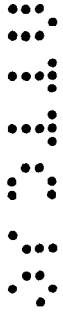
(k) $\frac{\bar{m}}{m_0} = 0.57$; $\frac{\bar{H}_t}{H_0} = 0.66$; time, 5.0 seconds.



L-74344

Figure 10.- Continued.

~~CONFIDENTIAL~~



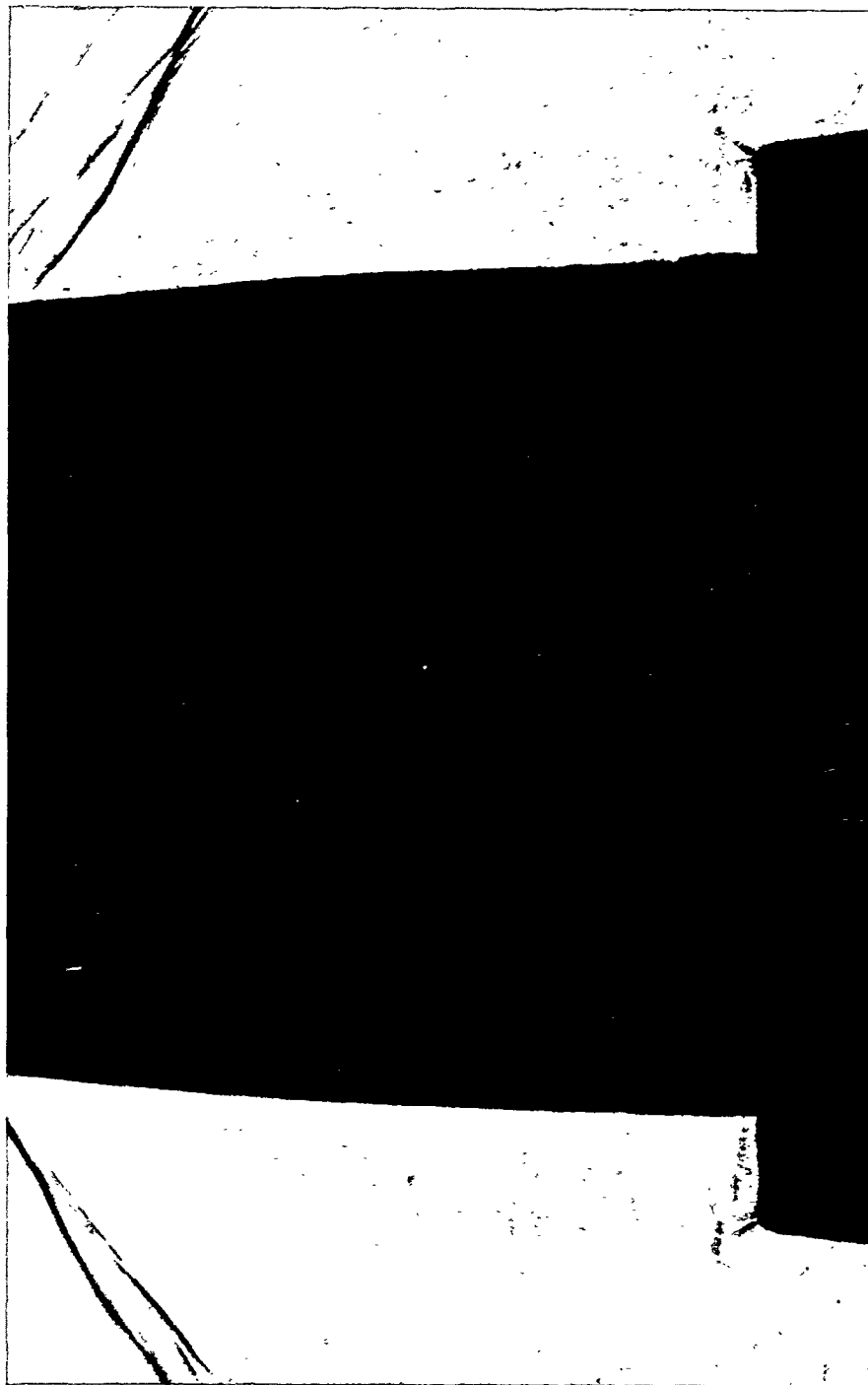
(2) $\frac{\bar{m}}{m_0} = 0.54; \frac{\bar{H}_t}{H_0} = 0.66; \text{time, } 5.5 \text{ seconds.}$



L-74345

Figure 10.- Continued.





(m) $\frac{\bar{m}}{m_0} = 0.51$; $\frac{\bar{H}_t}{H_0} = 0.66$; time, 6.0 seconds.



Figure 10.- Continued.

L-74346



(n) $\frac{\bar{m}}{m_0} = 0.48$; $\frac{\bar{H}_t}{H_0} = 0.66$; time, 6.5 seconds.



L-74347

Figure 10.- Concluded.

~~CONFIDENTIAL~~

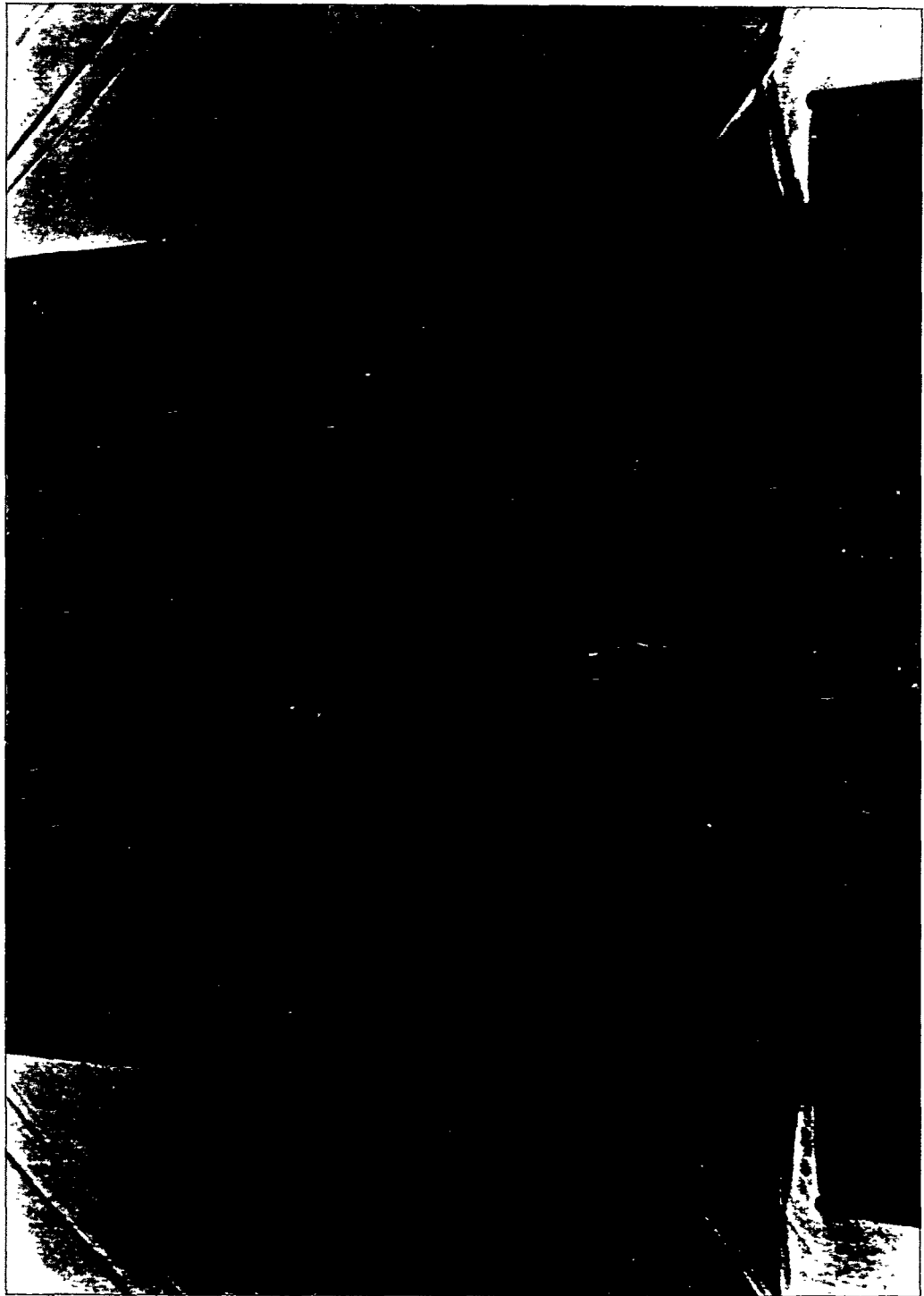


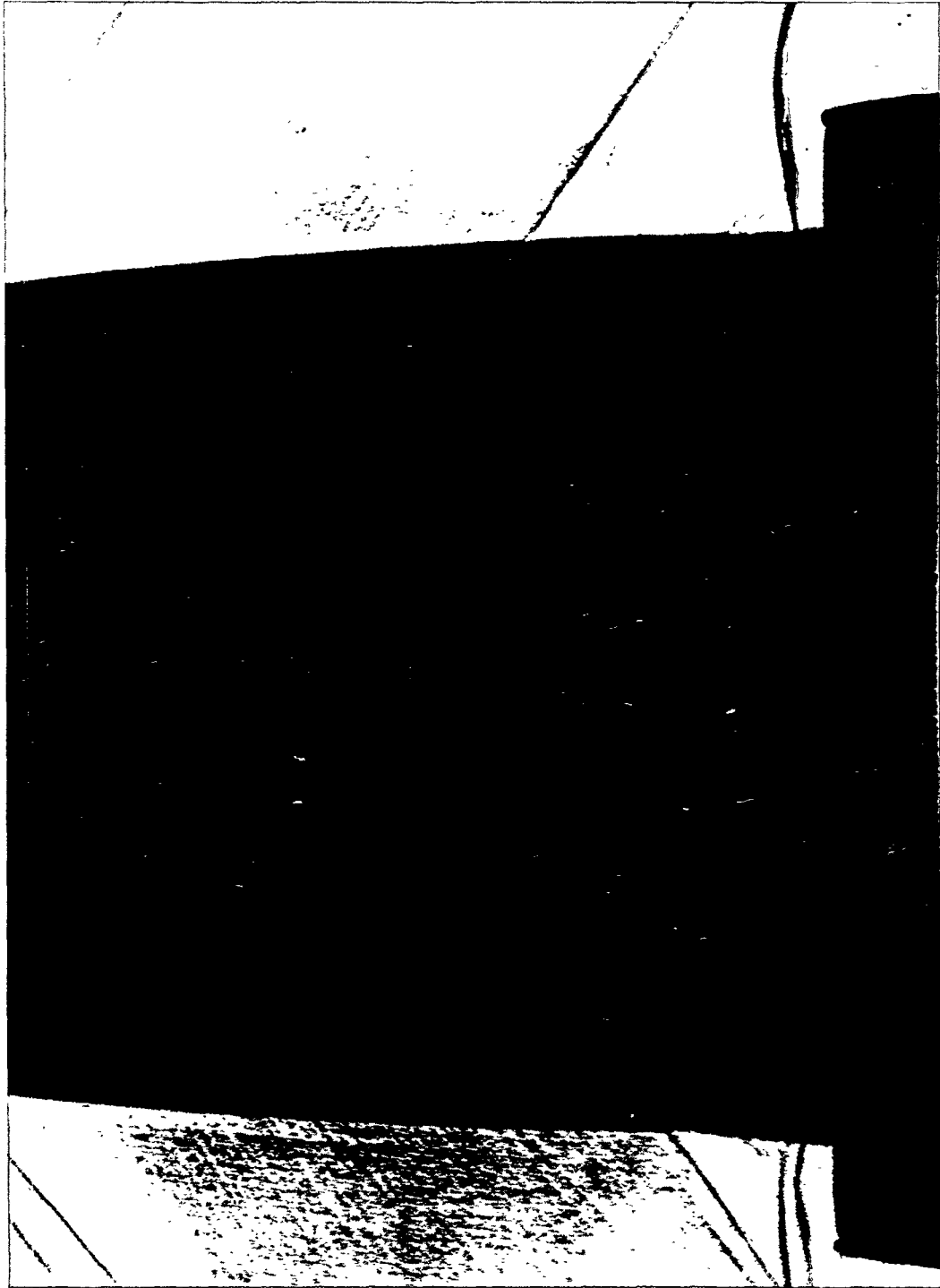
Figure 11.- Sample shadowgraph of unsteady flow with nose B. $M_0 = 1.55$;

$$\frac{\bar{m}}{m_0} = 0.60; \frac{\bar{H}_t}{H_0} = 0.58.$$



L-74348

~~CONFIDENTIAL~~



L-74349

Figure 12.- Sample shadowgraph of unsteady flow with nose C. $M_0 = 1.55$;

$$\frac{\bar{m}}{m_0} = 0.67; \frac{\bar{H}_t}{H_0} = 0.64.$$

SECURITY INFORMATION

NASA Technical Library



3 1176 01438 5653

~~CONFIDENTIAL~~